Evolution of structural dynamics in cesium lead halide perovskite colloidal nanocrystals from temperature-controlled synthesis [REE]

Special Collection: Festschrift in honor of Louis E. Brus

Gopi Adhikari ⑩ ; Bo Zhang ⑩ ; Yinsheng Guo **■** ⑩

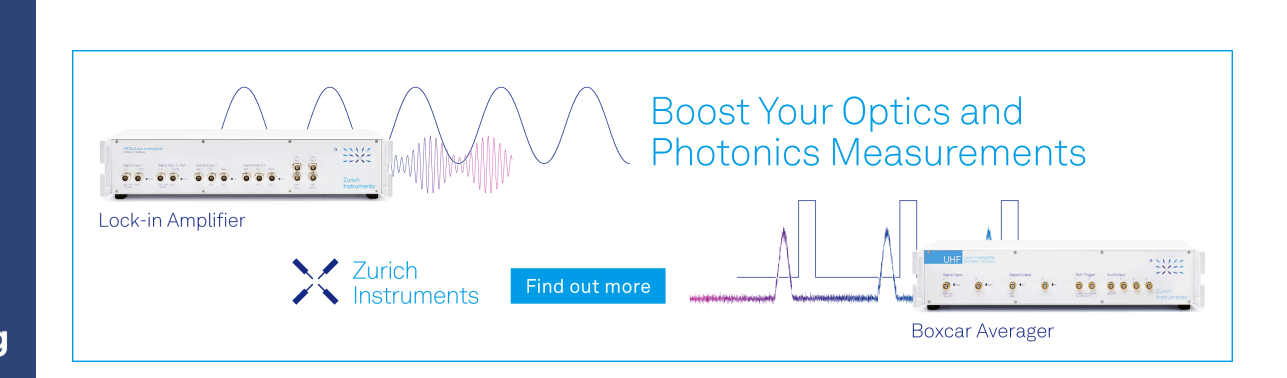


J. Chem. Phys. 160, 204702 (2024)

https://doi.org/10.1063/5.0206402









Evolution of structural dynamics in cesium lead halide perovskite colloidal nanocrystals from temperature-controlled synthesis

Cite as: J. Chem. Phys. 160, 204702 (2024); doi: 10.1063/5.0206402

Submitted: 1 March 2024 • Accepted: 6 May 2024 •

Published Online: 22 May 2024







Gopi Adhikari, (D) Bo Zhang, (D) and Yinsheng Guo^{a)} (D)







AFFILIATIONS

Department of Chemistry, University of Nebraska-Lincoln, Lincoln, Nebraska 68526, USA

Note: This paper is part of the JCP Festschrift in Honor of Louis E. Brus.

a) Author to whom correspondence should be addressed: yinshengguo@unl.edu

ABSTRACT

Halide perovskite nanocrystals are at the forefront of materials research due to their remarkable optoelectronic properties and versatile applications. While their lattice structure and optical properties have been extensively investigated for the structure-property correlation, their lattice dynamics, the physical link between the lattice structure and optoelectronic properties, has been much less visited. We report the evolution of structural dynamics of a series of cesium lead halide perovskite nanocrystals whose size and morphology are systematically varied by synthesis temperature. Low-frequency Raman spectroscopy uncovers the nanocrystals' structural dynamics, including a relaxational spectral continuum from ligand librations and a phonon spectrum evolving with nanocrystal size. As the size of nanocrystals increases, their phonon spectrum becomes more intense, and their spectral weights redistribute with new first- and second-order modes being activated. The linewidth of the observed phonon modes generally broadens as the nanocrystal grows larger, an interesting deviation from the established phonon confinement model. We suggest that strong confinement and truncation of the lattice and ligands anchoring on the surface might lead to pinning of the lattice dynamics at nanoscale. These findings offer new insights into the bulk-nano-transition in halide perovskite soft

Published under an exclusive license by AIP Publishing. https://doi.org/10.1063/5.0206402

INTRODUCTION

Lead halide perovskites (LHPs) have emerged as a stellar class of solution processed semiconductor materials opening new grounds from photovoltaics and broad field of optoelectronics.¹ Bulk LHPs now competes and complements silicon in photovoltaic applications.2 Their device performance enabled by outstanding electronic properties is fundamentally surprising for an ionic semiconductor processed at low temperatures, which opens new scientific grounds in understanding the structural origin of exceptional electronic properties.^{3,4} In its nanocrystalline form, the LHP nanocrystals (NCs) have shown intriguing properties with exciting applications ranging from renewable energy and optoelectronics to quantum information science.5-7 LHP NCs possess even more structural defects and labile chemistry than their bulk counterpart, yet they exhibit robust high quantum yield in photoluminescence (PL) among many other appealing optoelectronic properties. The nature of the nanoconfined lattice and

its surface states are long-standing questions for scientists and

Lattice dynamics plays a critical role in defining the optoelectronic and structural properties of bulk LHPs. Large amplitude highly anharmonic nuclear motions have been recognized as a unique feature distinguishing halide perovskite semiconductors apart from conventional counterparts. 8-11 As the crystal size shrinks and transitions into the nanoscale, the structure-property relationship becomes more complex and interesting as the system is strongly modified by quantum confinement, predominance of interfaces, as well as altered dielectric environments. 12,13 While the structure and optoelectronic properties of LHP NCs have received the spotlight of the research community and have been extensively studied, the lattice dynamics of these nanocrystals have received much less investigation.

In this work, we present a study of the evolution of structural dynamics in cesium lead halide perovskite colloidal nanocrystals. A series of prototypical halide perovskite nanocrystals were grown from colloidal solutions, in which temperature sensitively controlled their size and morphology progression from nanowires to nanoplates and nanocubes. Basic knowledge of the evolution of lattice dynamics from nano to bulk provides insights to bridge the gap in our understanding of perovskite nanocrystals' chemical structure and optoelectronic properties.

RESULTS AND DISCUSSION

Lattice structure

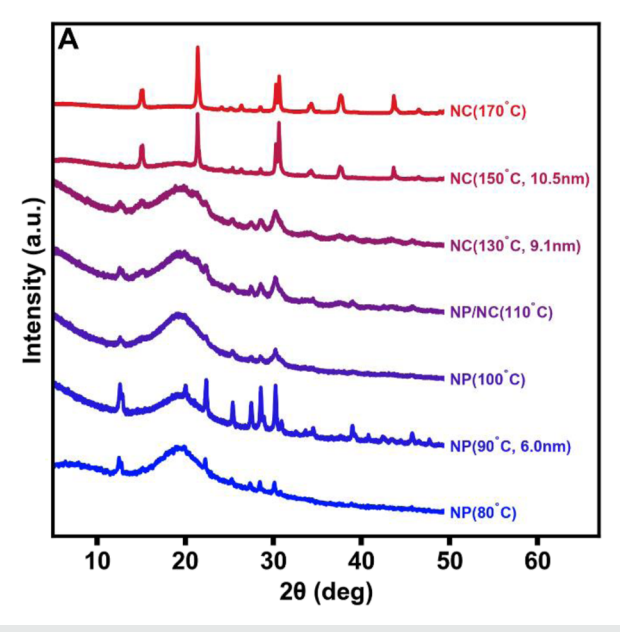
The CsPbBr3 nanocrystals were synthesized following the original report by Protesescu et al.14 and the adapted method by Bekenstein et al. 15 Growth temperature was utilized as the key parameter to control and size and morphology distribution of colloidal crystals. To elucidate the impact of reaction temperature on the lattice structure of the nanocrystals, we measured the x-ray diffraction (XRD) patterns of the CsPbBr₃ nanocrystals, as shown in Fig. 1(a). Bulk CsPbBr₃ exists in the orthorhombic phase (Pnma) at room temperature. The XRD diffractograms of nanocrystals synthesized at high temperatures (T > 150 $^{\circ}$ C) match well with that of the bulk CsPbBr3 and exhibit strong peaks at ~15.2°, 21.5°, and 30.7° associated with the (101), (121), and (202) planes, respectively. In this group of nanocrystals, the intensity of Bragg's peak corresponding to the plane (121) is relatively high compared with those of other peaks, indicating a preferential orientation of the nanocrystals in the XRD sample. The lattice parameters are calculated as a = 6.7 Å, b = 11.71 Å, and c = 11.78 Å. In the group of NCs synthesized at intermediate temperatures (80 °C < T < 150 °C), their XRD

diffractograms show a new set of peaks that differ from the orthorhombic CsPbBr3. This set of diffraction peaks indicate the presence of Cs4PbBr6 crystallites, which may result from the weak solubility of PbBr2 at low temperatures. Similar observations have been reported previously. 16 In the group of NCs synthesized at low temperatures (T < 80 $^{\circ}$ C), the particles were not grown sufficiently. The small particle size and high surface-area-to-volume ratio resulted in the amorphous ligands dominating in the XRD diffractograms (not shown). Overall, the diffraction peaks shift slightly toward higher diffraction angles as the growth temperature increases, which suggests a gradual shrinking of the unit cell. The diffraction peaks narrow as the reaction temperature increases, which indicates the formation of larger particles with increasing crystallinity.

Morphology

Transmission electron microscopy (TEM) measurements were carried out to study the effect of temperature on the morphology of as-synthesized CsPbBr $_3$ nanocrystal samples at various reaction temperatures, as shown in Figs. 1(b)–1(e). The morphology and size of the nanocrystals are sensitively controlled with the growth temperature. This temperature-dependent variation of nanocrystal morphology is not smooth and continuous; rather, a few types of qualitatively distinct growth behaviors are observed as growth temperature is varied, as we discuss below.

Reactions at high temperatures (130° C < T < 170° C) produce cube and cuboid nanocrystals. Reactions conducted at 130° C produce mostly symmetrical and monodisperse nanocubes with a



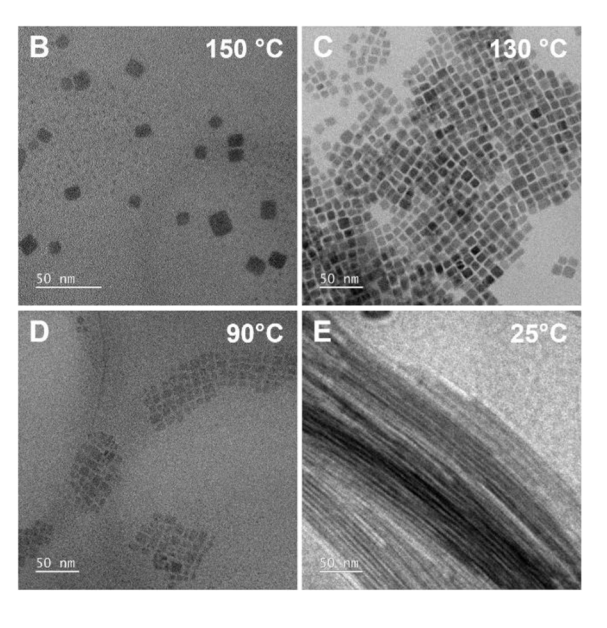


FIG. 1. Structure and morphology of $CsPbBr_3$ nanocrystals and their dependence on synthesis temperature. (a) X-ray diffractograms of $CsPbBr_3$ nanocrystals grown from 80 to 170 °C. NP: nanoplates, NC: nanocubes. (b) Transmission Electron Microscope (TEM) image of $CsPbBr_3$ nanocubes grown at 150 °C with an average characteristic size of 10.5 nm. (c) TEM image of $CsPbBr_3$ nanoplates formed at 130 °C with an average characteristic size of 9.1 nm. (d) TEM image of $CsPbBr_3$ nanoplates formed at 90 °C with an average characteristic size of 6.0 nm. (e) TEM image of $CsPbBr_3$ nanowires formed at 25 °C with an average width of 2.3 nm. Scale bars: 50 nm.

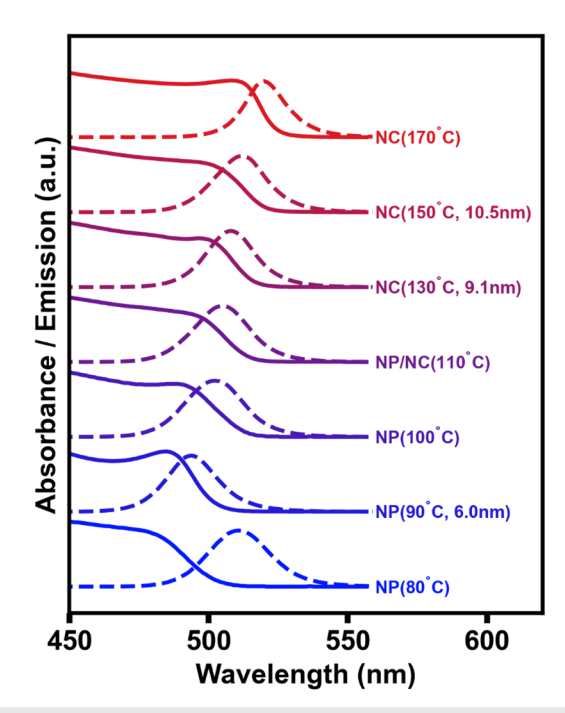


FIG. 2. Electronic spectra of CsPbBr₃ nanocrystals. Solid lines: absorption spectra. Dashed lines: photoluminescence spectra. The spectra are linearly scaled to set their minimum and maximum between 0 and 1 and vertically offset for clarity.

dimension of about 9.1 nm and having a green emission, as shown in Fig. 1(c). At elevated temperatures, the size of the nanocubes increases; at 150 °C, for instance, the size of the nanocubes reaches 10.5 nm [Fig. 1(b)], starting to lift quantum confinement. The monodispersity also noticeably decreases at elevated growth temperatures. The reactions at the temperature range of 25 °C < T < 130 °C tends to strongly favor asymmetric growth forming quasi-2D geometries. Figure 1(d) shows thus formed nanoplates at 90 °C with an average edge length of 6.0 nm. The ionic nature of the metathesis reaction dictates the rapid nucleation and growth kinetics of the resulting nanocrystals. In this process, the reaction temperature plays a critical role. At the reaction temperatures of 90 and 50 °C, thin nanoplates were detected along with well-ordered lamellar structures (average width ~2.7 nm). The reactions at a low temperature of 25 °C leads to the formation of thin and long nanowires with an average width of 2.3 ± 0.4 nm, which corresponds to ~4 unit cells, as shown in Fig. 1(e).

This morphological transformation steered by the growth temperature is likely due to the organic mesostructures that are present during nanocrystal growth. 17 The size and shape distribution of the colloidal assemblies of organic molecules sensitively depends on the solution temperature. During the nanocrystal growth period, they define the nanocrystals' access to the solutes as well as tune the interplay of interfacial energy and thus serve as growth directing soft templates. Similar soft templating mechanisms have been reported for wurtzite CdSe nanocrystals. Notwithstanding the rich structural variations displayed in the progression of growth temperature, the evolution of optical behaviors appears relatively simple. As the

growth temperature increases, the electronic transitions, probed by both absorption and emission, largely redshift from their quantum confined values and converge toward the bulk limit, as shown in Fig. 2. One exception is the emission of NCs grown at 80 °C, which appears to be redshifted from the expected position and shows up at ~510 nm. This individual case of blue absorption and anomalous shifted green emission suggests additional interactions in the photoexcited state of these NCs. A likely explanation is an unintended aggregation during the morphological transformation and sample preparation of NCs grown at 80 °C. Similar phenomena have been reported by Di Stasio $et\ al.^{19}$ They reported a concentration-dependent PL shift from the blue to the green spectral regions in CsPbBr3 nanowires and nanoplatelets, as isolated nanocrystals aggregate at high concentrations and in solid films.

To explore the size dependence of structural dynamics in $CsPbBr_3$ nanocrystals, we measured their vibrational spectra via low frequency Raman scattering. The results are shown in Figs. 3 and 4, which we discussed below.

Central peak (group i)

A first prominent feature in the low frequency Raman spectra of CsPbBr₃ NCs is a spectral continuum background, whose intensity increases as frequency approaches zero from both the Stokes and anti-Stokes sides. Hence, this spectral feature is phenomenologically named central peak. Heuristically, the central peak originates from physical processes that do not exhibit restoration force against external perturbations. Common examples include molecular motions, such as translation, rotation, and libration, in molecular liquids and polymers.²⁰ These are also the structural dynamic basis of dielectric relaxation.²¹ Severely overdamped nuclear motions in solids, including many ferroelectrics, also give rise to such prominent central peaks. 22-24 Intraband electronic processes in semiconductors and metals as well as in strongly correlated materials provide examples of central peaks of electronic origins. 25-27 In bulk halide perovskites, previous studies have shown that their lead-halide octahedral framework and A-site cation both display large amplitude highly anharmonic motion and give rise to a central peak. 10,11

Figure 3(a) shows the central peak observed in CsPbBr₃ NCs compared to that of the bulk crystal. In all cases, the spectra contain both the continuum background and vibrational peaks overlaid together. The relative weight of the relaxational spectral continuum decreases as the size of the nanocrystal increases. Meanwhile, the relative weight of the LHP vibrational spectrum increases as the size of the nanocrystal increases.

Ligands and lattice collective structural dynamics (group i)

A simple chemical interpretation of the relative weights' evolution comes from examining the surface-area-to-volume ratio in nanocrystals. We tentatively ascribe the origin of the relaxational response to the ligands on the nanocrystals' surface. The ligands pack on nanocrystal surfaces and form an interphase separating the nanocrystal cores in a solid film. Although the surface groups are expected to be largely anchored on the nanocrystal surface, one can envision their terminal groups to exhibit structural flexibility and display a librational motion in response to external fields. Such

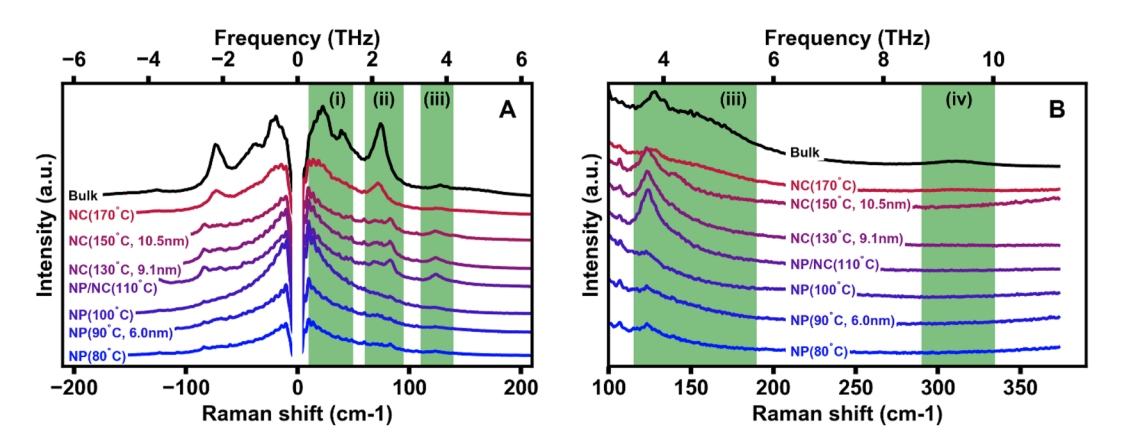


FIG. 3. Raman spectra of CsPbBr₃ nanocrystals grown under temperature control. (a) Stokes and anti-Stokes low frequency Raman spectra of the nanocrystals. (b) Highest frequency longitudinal optical phonon mode group and its second-order overtone. The spectra are linearly scaled to set their minimum and maximum between 0 and 1 and vertically offset for clarity. Bulk CsPbBr₃ Raman spectrum (black trace) is overlaid for comparison. NP: nanoplates, NC: nanocubes. The green bands highlight specific spectral regions and mode groups in discussion, labeled by Roman numerals: (i) low frequency collective spectral response from surface ligands and CsPbBr₃ lattice modes, (ii) CsPbBr₃ local structural modes, (iii) CsPbBr₃ highest energy LO modes, and (iv) CsPbBr₃ second-order modes.

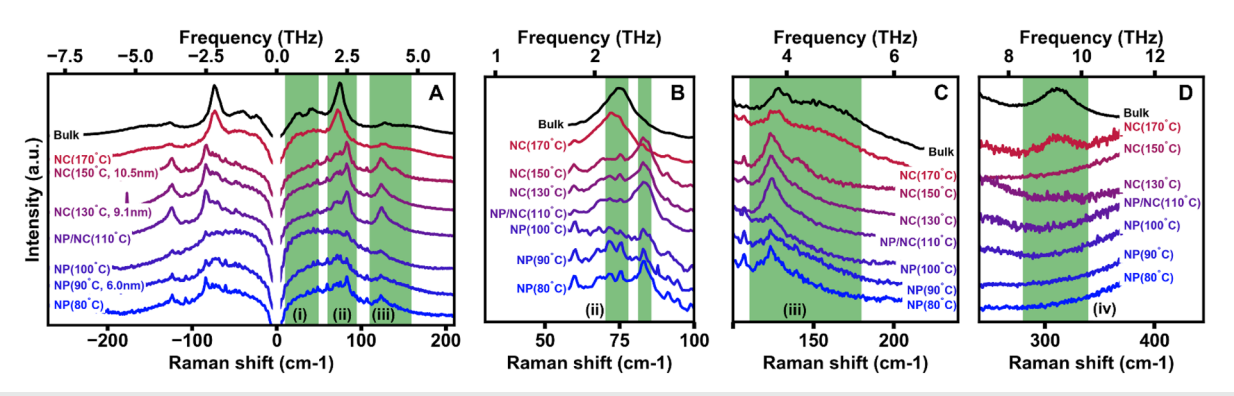


FIG. 4. Raman spectra of CsPbBr₃ nanocrystals, normalized against the Bose–Einstein factor. (a) Stokes and anti-Stokes low frequency Raman spectra of the nanocrystals. (b) Phonon mode group at 70–80 cm⁻¹. (c) Highest frequency longitudinal optical phonon mode group at 140–150 cm⁻¹. (d) Second-order mode at ~310 cm⁻¹. The spectra are linearly scaled to set their minimum and maximum between 0 and 1 and vertically offset for clarity. The bulk CsPbBr₃ Raman spectrum (black trace) is overlaid for comparison. NP: nanoplates, NC: nanocubes. The green bands highlight specific spectral regions and mode groups in discussion, labeled by Roman numerals: (i) low frequency collective spectral response from surface ligands and CsPbBr₃ lattice modes, (ii) CsPbBr₃ local structural modes, (iii) CsPbBr₃ highest energy LO modes, and (iv) CsPbBr₃ second-order modes.

a librational motion forms the structural dynamics basis of their dielectric relaxational response. In the case of nanocrystal thin films, the high surface-area-to-volume ratio means that the librational motion of surface ligands and the resulting dielectric relaxation play a significant role in their spectral response, along with the lattice dynamics of the nanocrystals. The smaller the nanocrystals, the larger their surface-area-to-volume ratio, hence the more weight their surface ligands' structural dynamics displays in the overall spectrum.

An alternative electronic interpretation of the evolution of relative spectral weights can be raised from the perspective of pre-resonance enhancement effect in Raman scattering. Proximity of the Raman excitation wavelength to a neighboring strong electronic transition can lead to an increase in the scattering cross section, known as the pre-resonance enhancement. As the size of the nanocrystals decreases, the band edge electronic transition blueshifts, moving further away from the excitation wavelength in the near infrared. As a result, one expects that the NCs' overall Raman scattering cross sections decrease as quantum confinement strengthens when measured with a fixed near infrared laser.

Bose-Einstein normalization

The central peak arises because the low frequency spectral response from the inherent structural dynamics, χ'' , is weighted by the Bose–Einstein (B–E) factor f_{BE} . In other words, the Raman

scattering cross section is determined by both the intrinsic susceptibility of the materials and a universal thermal population factor.³⁰ All thermal vibrational excitations are described by a Bose-Einstein distribution. Such a dependence can be simply expressed as $I \propto f_{BE} \chi''$. The Bose–Einstein factor is expressed as

$$f_{BE}(\omega,T) = \begin{cases} n_{BE}+1, & \omega>0, \\ n_{BE}, & \omega<0, \end{cases}$$

$$n_{BE}(\omega, T) = \frac{1}{\exp\left(\frac{\hbar\omega}{k_B T}\right) - 1}.$$

The Bose-Einstein factor behaves as a flat factor in the mid- to high-frequency spectral regions where the thermal Bose-Einstein population is negligible. In the low frequency region, however, it produces a non-negligible multiplier to the overall scattering cross section; this factor has a strong frequency dependence and diverges as the scattering frequency approaches zero.20 Its divergence at zero frequency renders finite inherent spectral responses into a peak. Thus, to reveal the underlying intrinsic spectral response, we normalize as measured low frequency Raman spectra using the Bose–Einstein factor following previously reported procedures.²⁰

Figure 4(a) shows the low frequency Raman spectra after normalization against the Bose-Einstein factor and reveals the underlying inherent spectral response in this region. This allows us to cleanly compare the relative weights between relaxational continuum and the LHP phonon spectrum. In the low temperature growth (T < 100 °C), the B-E normalized spectra show weak LHP phonon spectra overlaid on top of the strong relaxational continuum, as we discussed above. In the mid-temperature growth (100 °C < T < 150 °C), the LHP phonon spectra assume a more significant weight compared with the underlying relaxational continuum. In the high temperature growth (T ~ 170 °C), the LHP phonon spectrum becomes the dominant spectral feature on top of the relaxational continuum.

It is interesting to note that we also observe the rotational Raman spectra of N2 and O2 molecules in the air, which show up as sharp lines in the low frequency range, mostly visible below 100 cm⁻¹. These rotational lines have widths much narrower than any spectral feature in our materials, making them easily identifiable. These molecules are ubiquitous at stable levels, and their rotational spectra are well understood. These aspects render the air rotational lines an excellent internal reference standard for Raman scattering cross section discussions. Comparing the relative intensities of LHP phonon modes and the central peak vs the air rotational lines also reveals a strong increase in the inherent scattering cross section as the nanocrystal size increases.

Next, we turn to the phonon spectra of CsPbBr₃ NCs and its dependence on synthetic conditions. The phonon band structure, density of states, and spectra of halide perovskites have been well studied and discussed in the literature from both theoretical and experimental perspectives. 10,22,31-34 Briefly, the structural dynamics of simple A site cations, such as Cs, are largely located in the low frequency region ($v < 100 \text{ cm}^{-1}$), whereas the structural dynamics of lead halide octahedral framework spans a broader range from the highest optical phonon branches down to acoustic ranges. In the region above 100 cm⁻¹, the lead halide octahedral distortion assumes the most significant role in its spectral response.

Local structural dynamics at 70-80 cm⁻¹ (group ii)

From the phonon density of states perspective, the mode group around 70 cm⁻¹ has strong contributions from both A site cations and the BX6 octahedra.31 In the case of bulk CsPbBr3 at finite temperatures, it has been shown that the head-to-head motion of the Cs cation coupled with the Br octahedral distortion and rotation dominates the structural fluctuations at low frequencies. 10 Figure 4(b) shows a zoomed-in plot of the region around 70-80 cm⁻¹ where a prominent first-order phonon mode group is observed in CsPbBr₃ NCs. Aside from an increase in scattering cross sections as NCs increase in size, the spectral weight distribution in this group shifts with nanocrystal size and shows three types of behaviors. At low synthesis temperatures (T < 100 $^{\circ}$ C), this mode group is overall quite weak; the main peak occurs at $\sim 80 \text{ cm}^{-1}$. At intermediate synthesis temperatures (100 °C < T < 150 °C), this mode group gains significant intensity while maintaining a similar distribution of spectral weights. The main peak at ~80 cm⁻¹ broadens. At high synthetic temperatures (T > 150 °C), this mode group further gains intensity and its spectral weight downshifts and peaks at ~70 cm⁻¹. Interestingly, the linewidth increases as nanocrystal size increases, trending toward convergence with the broad linewidth in bulk crystals. A linewidth broadening as nanocrystal size increases is an unexpected trend for nanoconfined phonons. Such a behavior is seen again in other spectral regions and discussed in detail after surveying all prominent spectral features.

Highest energy LO phonons (group iii)

Figure 4(c) shows the CsPbBr₃ NCs Raman spectra normalized against the Bose-Einstein factor, zoomed in at around 150 cm⁻¹. This mode group corresponds to the highest energy longitudinal optical (LO) phonon bands in bulk LHPs. In this spectral range, phonon modes originate from the distortional motion of networked lead halide octahedra.³¹ It has been shown that these highest energy LO phonons interact strongly with charge carriers in bulk LHPs and play a critical role in bridging charge carrier-lattice interactions in diverse scenarios from hot carrier cooling, polaron formation, band edge carrier relaxation, to carrier scattering in charge transport. Currently, there are strong efforts in developing LHP nanocrystals toward energy, optoelectronic, and quantum information applications, in which electron-phonon interactions in nano-confined LHP lattice provide the underpinnings of their device operation. Thus, there is a strong motivation to reveal the size dependence of these

The size-dependent spectral behaviors of the highest LO phonons in CsPbBr3 NCs can be largely categorized into three groups, similar to the lower frequency first-order modes. (1) At low synthetic temperatures (T < 100 °C), this mode group is very weak compared with the continuum background. The main peak is located at ~123 cm⁻¹, with a shoulder peak on the low frequency side around ~115 cm⁻¹. (2) At intermediate synthetic temperatures (100 °C < T < 150 °C), this mode group becomes much more prominent. The main peak remains at 125 cm⁻¹. The low frequency shoulder peak shows negligible intensity in comparison. On the high frequency side, a new broad shoulder peak appears at about $140~\rm cm^{-1}$. (3) As the synthetic temperature increases (T > $150~\rm ^{\circ}C$) and as the nanocrystals further grow, this shoulder peak increases in both its intensity and width. In the high end of the synthetic temperature, this shoulder peak gains intensity, upshifts, and broadens significantly. The overall spectral weights of the LO phonon group upshift, extending beyond $150~\rm cm^{-1}$, and appear to be comparable with the highest energy LO phonon mode group in bulk CsPbBr3.

Second-order mode (group iv)

We next turn to investigate the size-dependent spectral behavior of the mode observed at $\sim 310~{\rm cm}^{-1}$, as shown in Fig. 4(d). This mode was previously assigned as a torsional mode of ${\rm CH_3NH_3}^+$ (methylammonium, MA) ion in hybrid halide perovskites. 33,38 Its persistent appearance in all-inorganic CsPbBr₃, at a location consistent with the mode observed in MAPbBr₃, suggests that this mode does not involve MA motion. Comparing mode frequencies within a simple harmonic oscillator model across different A-site cations and X halide ions, we suggest a reassignment of this mode to a second-order overtone or combination mode based on the highest LO phonon group. 39

The spectral behavior of this second-order mode markedly differs from that of the first-order LO modes discussed above. First, the appearance of second-order mode correlates with the appearance of the broad mode group around 150 cm⁻¹ from NCs grown at the highest temperatures [Figs. 4(c) and 4(d)]. Their correlated appearances also support our assignment of the second-order mode. Second, the second-order mode shows a well-defined and simple line shape; neighboring first-order modes in group iii possess much smaller spectral weights in the second order. The varied weights of different phonons in the higher order modes originate from mode-dependent electron-phonon coupling strengths. A particular phonon branch in the highest energy phonon group couples with the electronic states in CsPbBr3 and thus outweighs other phonon modes in the neighboring frequency range. 35,40 Third, this secondorder mode appears much later in the NCs' size progression defined by their synthesis temperature from low to high. This second-order mode remains silent in NCs grown at all lower temperatures; it appears only in NCs grown at the highest temperature ($T \sim 170$ °C) with the largest size (>10 nm), above the exciton Bohr radius of bulk CsPbBr₃ and lifting quantum confinement. Our observations suggest that nanoscale confinement of the halide perovskite lattice alters the phonon spectrum and likely redefines carrier-lattice interactions.

Phonon linewidth broadening with increasing nanocrystal size

So far, we have surveyed the behaviors of CsPbBr₃ NCs' prominent phonon modes in four spectral regions. Structural dynamics of nanocrystals are often understood within the framework of phonon confinement models. Briefly, nanoscale truncation of the crystal lattice brings uncertainty in the crystal momentum and modifies the spectral line shapes. The resulting spectral line shape is expected to be a sum of a distribution of Lorentzians weighted by a function describing the uncertainty in momentum space, resulting in a line shape broadening. In addition, the broadened sampling of

phonon dispersions in momentum space often, though not always, produces softened vibrations from the weighted summation. Such a phonon confinement model has been widely used in the study of semiconductor nanocrystals, such as Si, 41,42 Ge, 43 GaAs, 42 with 3D bulk lattice structures, as well as 2D van der Waals semiconductor MoS₂. 44 As the crystal size decreases to the few nanometer regime, typical expectations are that nanoscale confinement broadens and softens the phonon spectra.

The CsPbBr₃ NCs probed in this work show surprising behaviors in this context. Contrary to the phonon confinement behavior, the first-order phonon modes of CsPbBr₃ NCs broaden as their size increases in the few nanometer range. As the size of NCs grows beyond ~10 nm, the phonon spectra start to converge with that of the bulk crystal, via a continued broadening of the phonon modes. In bulk CsPbBr3, phonon anharmonic interactions in a soft and fluctuating lattice give rise to the observed mode broadening. We postulate that in the few-nanometer to few-unit-cell size regime, such anharmonic structural dynamics might be suppressed in a confined lattice or pinned by ligand bonding to the surface lattice. One possible mechanism is that the lead halide octahedral network itself is inherently pinned under strong structural truncation. In other words, the anharmonic structural fluctuations possibly entail the lead halide octahedral framework to be extended in three dimensions to be active. In addition, bonding to surface ligands might contribute to pinning the surface lattice of the underlying lead halide framework. As the surface-area-to-volume ratio increases as the size of NCs decreases, the surface pinning could play an increasingly important role in governing the structural dynamics of the nanocrystal core. Interestingly, recent work on nanocrystal structural dynamics has revealed a crossover from confined phonon to molecular vibration pictures at 2.1 nm using atomically precise cadmium selenide quantum dots.45

CONCLUSION

In conclusion, we present a correlated study of size and morphology dependence of structural dynamics in halide perovskite colloidal nanocrystals. Reaction temperature sensitively steers the growth trajectory of CsPbBr3 colloidal nanocrystals switching from nanocubes formed at high temperatures to nanoplates formed at intermediate temperatures and to nanowires formed at low temperatures. Despite the structural variety and diversity displayed under the temperature control parameter, the evolution of optical behaviors appears straightforward. As the growth temperature increases, the electronic transitions redshift from their quantum confined values and converge with the bulk limit. Low frequency Raman spectroscopy reveals the structural dynamics of the nanocrystals in the solid state. A relaxational spectral continuum originating from the ligand librations is prominently present in nanocrystal random solids. The halide perovskite phonon spectrum is significantly modified by the confinement and morphology of the nanocrystals. Surprisingly, the evolution of structural dynamics deviates from typical expectations of a phonon confinement model and shows a continued broadening as nanocrystals' size increases. Understanding the halide perovskite nanocrystal structural dynamics provides crucial insights into engineering perovskite quantum dots for optoelectronic and quantum applications.

EXPERIMENTAL METHODS

Synthesis of $CsPbBr_3$ nanocrystals (NCs), microwires, and bulk crystals

Preparation of cesium oleate

 $0.4~g~Cs_2CO_3$ (99%, Aldrich) was loaded into a 100 ml flask along with 15 ml octadecene (ODE) and 1.2 ml oleic acid (OA). The mixture was degassed under vacuum at 120 $^{\circ}C$ for 1 h and then heated under N_2 to 150 $^{\circ}C$ until all Cs_2CO_3 reacted with OA.

Synthesis of CsPbBr3 nanocrystals

PbBr₂ (0.069 g, 99.998%, Alfa Aesar) was loaded into a 50 ml flask along with ODE (5 ml), oleylamine (0.5 ml, OLA), and OA (0.5 ml) and then dried under vacuum for 1 h at 120 $^{\circ}$ C. After complete solubilization of the PbBr₂ salt under N₂ atmosphere, the solution temperature was changed to selected value in the range of 25–170 $^{\circ}$ C. A hot (~100 $^{\circ}$ C) Cs-oleate solution (0.4 ml) was quickly injected, and the reaction mixture was immediately cooled with an ice-water bath. For low temperature batches (≤50 $^{\circ}$ C), the reaction continued for 1 h with vigorous stirring.

After the reaction, the NCs were extracted from the crude solution by centrifugation at 8500 rpm for 10 min. For low temperature batches (growth temperature \leq 50 $^{\circ}$ C), centrifugation was carried out at 15 000 rpm. After centrifugation, the supernatant was discarded, and the precipitated NCs were redispersed with hexane forming stable colloidal solutions. Subsequently, the colloidal solution was kept still in a vial for several days. Slowly formed aggregates settled to the bottom of the vial. The supernatant was extracted carefully without shaking the vial and centrifuged again at 13 000 rpm for 10 min. The NCs precipitated from the second centrifugation were collected, redispersed in the hexane, and used for further characterization.

Synthesis of CsPbBr₃ microwires and bulk crystals

CsPbBr3 microwires were synthesized using a space-confined evaporative growth method at room temperature. Briefly, 0.45 mmol of CsBr and 0.45 mmol PbBr2 were mixed with 1 ml of dimethyl sulfoxide (DMSO) and stirred vigorously on a hot plate at 65 °C for 4-5 h. Afterward, the solution was cooled to room temperature and filtered using a <0.22 μm filter. Two glass substrates (~25 \times 25 × 1 mm³) were cleaned ultrasonically in DI water, ethanol, and isopropanol sequentially for 15 min each step and dried using a hot air blow. Then, a 5 µl precursor solution was dropped onto a cleaned glass substrate using a pipette and covered with another identical glass substrate rotated diagonally. The precursor solution was spread throughout the substrate surface and filled the space between two substrates. The assembly was kept unperturbed overnight. Multiplemillimeter long single-crystal CsPbBr₃ wires grew between the glass substrates. The length of the crystal wires can be controlled by varying the growth time (~0.5 cm in two days). At the end of the crystal growth, the glass substrates were carefully separated. The wires were washed with hexane and dried under a nitrogen blow. Bulk crystals were grown from the same precursor solution inside a vial unperturbed with slow evaporative removal of the solvent over a course of more than two weeks. The CsPbBr3 microwires and bulk crystals were both grown at room temperature under ambient conditions.

Characterizations

Structural characterization

X-ray diffraction was measured using a PANalytical Empyrean Diffractometer equipped with a PIXcel3D detector with CuKα1 radiation, $\lambda = 1.540\,598\,0$ Å operated with 45 kV and 40 mA, and at an angular range (2θ) with a step size of 0.0131°. The transmission electron microscopy (TEM) images were obtained using an FEI Tecnai Osiris (S)TEM operated at 200 kV; the exposure time was 0.8 s.

Solution phase optical characterizations

Colloidal solution samples were prepared by diluting 30 μ l stock colloidal solutions in 3 ml toluene. The emission/excitation spectra of as-prepared colloidal solution samples were measured using a fluorimeter (Shimadzu RF-5301PC). The UV–visible absorption spectra were collected using a UV–Vis spectrophotometer (Shimadzu 2501 UV–VIS, HP 8452 UV–VIS).

Low-frequency Raman spectroscopy

Colloidal solutions of nanocrystals were spin-coated (EZ4 spin coater) into thin films for low-frequency Raman spectroscopy measurements. In the case of nanocrystal samples synthesized at lower temperatures, the obtained films were thin. A sharp blade was used to collect and pack nanocrystal random solids into a thick film at the center of the substrate.

A low-frequency Raman spectroscopy measurement was performed on a home-built Raman microscope system. The excitation laser centered at 830 nm was provided by a diode laser module stabilized by volume holographic grating (Ondax). The diode laser module also housed volume holographic grating notch filter sets for Raman signal filtering and laser line rejection. The excitation beam was coupled into a home-built microscope via free space. A microscope objective (Nikon Plan Fluor ELWD 60x NA 0.70) focused the excitation laser onto the samples and collected the backscattered signal. The Raman signals were filtered and fiber-coupled onto the entrance plane of a spectrometer (Princeton Instruments IsoPlane 320), dispersed by a 1200 grooves/mm gratin, and imaged onto a thermal electrically cooled CCD (Princeton Instruments, PIXIS 400). The typical laser power was ~60 mW.

ACKNOWLEDGMENTS

This work was supported by the National Science Foundation/EPSCoR RII Track-1: Emergent Quantum Materials and Technologies (EQUATE), Award No. OIA-2044049. Y.G. acknowledges support by the National Science Foundation under Award No. DMR-2339721. The research was performed, in part, in the Nebraska Nanoscale Facility: National Nanotechnology Coordinated Infrastructure and the Nebraska Center for Materials and Nanoscience (NCMN) and Nano-Engineering Research Core Facility (NERCF), which are supported by the National Science Foundation under Award No. ECCS: 2025298, and the Nebraska Research Initiative.

AUTHOR DECLARATIONS

Conflict of Interest

The authors have no conflicts to disclose.

Author Contributions

Gopi Adhikari: Data curation (equal); Formal analysis (equal); Investigation (equal); Methodology (equal); Writing – original draft (equal). Bo Zhang: Formal analysis (equal); Investigation (equal); Writing – original draft (equal). Yinsheng Guo: Conceptualization (equal); Formal analysis (equal); Funding acquisition (equal); Investigation (equal); Project administration (equal); Supervision (equal); Writing – original draft (equal); Writing – review & editing (equal).

DATA AVAILABILITY

The data that support the findings of this study are available from the corresponding author upon reasonable request.

REFERENCES

- ¹C. C. Stoumpos and M. G. Kanatzidis, "The renaissance of halide perovskites and their evolution as emerging semiconductors," Acc. Chem. Res. **48**(10), 2791–2802 (2015).
- ²E. Aydin, T. G. Allen, M. De Bastiani, A. Razzaq, L. Xu, E. Ugur, J. Liu, and S. De Wolf, "Pathways toward commercial perovskite/silicon tandem photovoltaics," Science 383(6679), eadh3849 (2024).
- ³D. A. Egger, A. Bera, D. Cahen, G. Hodes, T. Kirchartz, L. Kronik, R. Lovrincic, A. M. Rappe, D. R. Reichman, and O. Yaffe, "What remains unexplained about the properties of halide perovskites?," Adv. Mater. **30**(20), 1800691 (2018).
- ⁴Q. A. Akkerman and L. Manna, "What defines a halide perovskite?," ACS Energy Lett. 5(2), 604–610 (2020).
- ⁵Q. A. Akkerman, G. Rainò, M. V. Kovalenko, and L. Manna, "Genesis, challenges and opportunities for colloidal lead halide perovskite nanocrystals," Nat. Mater. 17(5), 394–405 (2018).
- ⁶H. Utzat, W. Sun, A. E. K. Kaplan, F. Krieg, M. Ginterseder, B. Spokoyny, N. D. Klein, K. E. Shulenberger, C. F. Perkinson, M. V. Kovalenko, and M. G. Bawendi, "Coherent single-photon emission from colloidal lead halide perovskite quantum dots," Science 363(6431), 1068–1072 (2019).
- ⁷A. Dey, J. Ye, A. De, E. Debroye, S. K. Ha, E. Bladt, A. S. Kshirsagar, Z. Wang, J. Yin, Y. Wang, L. N. Quan, F. Yan, M. Gao, X. Li, J. Shamsi, T. Debnath, M. Cao, M. A. Scheel, S. Kumar, J. A. Steele, M. Gerhard, L. Chouhan, K. Xu, X. Wu, Y. Li, Y. Zhang, A. Dutta, C. Han, I. Vincon, A. L. Rogach, A. Nag, A. Samanta, B. A. Korgel, C.-J. Shih, D. R. Gamelin, D. H. Son, H. Zeng, H. Zhong, H. Sun, H. V. Demir, I. G. Scheblykin, I. Mora-Seró, J. K. Stolarczyk, J. Z. Zhang, J. Feldmann, J. Hofkens, J. M. Luther, J. Pérez-Prieto, L. Li, L. Manna, M. I. Bodnarchuk, M. V. Kovalenko, M. B. J. Roeffaers, N. Pradhan, O. F. Mohammed, O. M. Bakr, P. Yang, P. Müller-Buschbaum, P. V. Kamat, Q. Bao, Q. Zhang, R. Krahne, R. E. Galian, S. D. Stranks, S. Bals, V. Biju, W. A. Tisdale, Y. Yan, R. L. Z. Hoye, and L. Polavarapu, "State of the art and prospects for halide perovskite nanocrystals," ACS Nano 15, 10775 (2021).
- ⁸C. Katan, A. D. Mohite, and J. Even, "Entropy in halide perovskites," Nat. Mater. 17(5), 377–379 (2018).
- ⁹K. Miyata and X.-Y. Zhu, "Ferroelectric large polarons," Nat. Mater. 17(5), 379–381 (2018).
- ¹⁰O. Yaffe, Y. Guo, L. Z. Tan, D. A. Egger, T. Hull, C. C. Stoumpos, F. Zheng, T. F. Heinz, L. Kronik, M. G. Kanatzidis, J. S. Owen, A. M. Rappe, M. A. Pimenta, and L. E. Brus, "Local polar fluctuations in lead halide perovskite crystals," Phys. Rev. Lett. 118(13), 136001 (2017).

- ¹¹A. N. Beecher, O. E. Semonin, J. M. Skelton, J. M. Frost, M. W. Terban, H. Zhai, A. Alatas, J. S. Owen, A. Walsh, and S. J. L. Billinge, "Direct observation of dynamic symmetry breaking above room temperature in methylammonium lead iodide perovskite," ACS Energy Lett. 1(4), 880–887 (2016).
- ¹² A. L. Efros and L. E. Brus, "Nanocrystal quantum dots: From discovery to modern development," ACS Nano 15(4), 6192–6210 (2021).
- ¹³ J. Owen and L. Brus, "Chemical synthesis and luminescence applications of colloidal semiconductor quantum dots," J. Am. Chem. Soc. 139(32), 10939–10943 (2017).
- ¹⁴L. Protesescu, S. Yakunin, M. I. Bodnarchuk, F. Krieg, R. Caputo, C. H. Hendon, R. X. Yang, A. Walsh, and M. V. Kovalenko, "Nanocrystals of cesium lead halide perovskites (CsPbX₃, X = Cl, Br, and I): Novel optoelectronic materials showing bright emission with wide color gamut," Nano Lett. **15**(6), 3692–3696 (2015).
- ¹⁵Y. Bekenstein, B. A. Koscher, S. W. Eaton, P. Yang, and A. P. Alivisatos, "Highly luminescent colloidal nanoplates of perovskite cesium lead halide and their oriented assemblies," J. Am. Chem. Soc. 137(51), 16008–16011 (2015).
- ¹⁶ A. Kostopoulou, M. Sygletou, K. Brintakis, A. Lappas, and E. Stratakis, "Low-temperature benchtop-synthesis of all-inorganic perovskite nanowires," Nanoscale 9(46), 18202–18207 (2017).
- ¹⁷W. Sun, R. Yun, Y. Liu, X. Zhang, M. Yuan, L. Zhang, and X. Li, "Ligands in lead halide perovskite nanocrystals: From synthesis to optoelectronic applications," Small 19(11), 2205950 (2023).
- ¹⁸J. S. Son, X.-D. Wen, J. Joo, J. Chae, S. Baek, K. Park, J. H. Kim, K. An, J. H. Yu, S. G. Kwon, S.-H. Choi, Z. Wang, Y.-W. Kim, Y. Kuk, R. Hoffmann, and T. Hyeon, "Large-scale soft colloidal template synthesis of 1.4-nm thick CdSe nanosheets," Angew. Chem., Int. Ed. 48(37), 6861–6864 (2009).
- ¹⁹F. Di Stasio, M. Imran, Q. A. Akkerman, M. Prato, L. Manna, and R. Krahne, "Reversible concentration-dependent photoluminescence quenching and change of emission color in CsPbBr₃ nanowires and nanoplatelets," J. Phys. Chem. Lett. **8**(12), 2725–2729 (2017).
- ²⁰S. Sun, D. T. N. Rathnayake, and Y. Guo, "Asymmetrical spectral continuum between anti-Stokes and Stokes scattering revealed in low-frequency surface-enhanced Raman spectroscopy," J. Phys. Chem. C 126(27), 11193–11200 (2022).
- ²¹ G. G. Raju, *Dielectrics in Electric Fields*, 2nd ed. (Taylor & Francis, CRC, 2016).
 ²² M. Menahem, N. Benshalom, M. Asher, S. Aharon, R. Korobko, O. Hellman, and O. Yaffe, "Disorder origin of Raman scattering in perovskite single crystals," Phys. Rev. Mater. 7(4), 044602 (2023).
- ²³ J. P. Sokoloff, L. L. Chase, and D. Rytz, "Direct observation of relaxation modes in KNbO₃ and BaTiO₃ using inelastic light scattering," Phys. Rev. B **38**(1), 597–605 (1988).
- ²⁴I. G. Siny, S. G. Lushnikov, R. S. Katiyar, and E. A. Rogacheva, "Central peak in light scattering from the relaxor ferroelectric PbMg_{1/3}Nb_{2/3}O₃," Phys. Rev. B **56**(13), 7962–7966 (1997).
- ²⁵B. Fluegel, A. V. Mialitsin, D. A. Beaton, J. L. Reno, and A. Mascarenhas, "Electronic Raman scattering as an ultra-sensitive probe of strain effects in semiconductors," Nat. Commun. 6(1), 7136 (2015).
- ²⁶Y. S. Ponosov and S. V. Streltsov, "Measurements of Raman scattering by electrons in metals: The effects of electron-phonon coupling," Phys. Rev. B 86(4), 045138 (2012).
- 27 T. P. Devereaux and R. Hackl, "Inelastic light scattering from correlated electrons," Rev. Mod. Phys. 79(1), 175–233 (2007).
- ²⁸ K. Miyata, T. L. Atallah, and X.-Y. Zhu, "Lead halide perovskites: Crystal-liquid duality, phonon glass electron crystals, and large polaron formation," Sci. Adv. 3(10), e1701469 (2017).
- ²⁹ P. Guo, Y. Xia, J. Gong, C. C. Stoumpos, K. M. McCall, G. C. B. Alexander, Z. Ma, H. Zhou, D. J. Gosztola, J. B. Ketterson, M. G. Kanatzidis, T. Xu, M. K. Y. Chan, and R. D. Schaller, "Polar fluctuations in metal halide perovskites uncovered by acoustic phonon anomalies," ACS Energy Lett. 2(10), 2463–2469 (2017).
- ³⁰W. H. Weber and R. Merlin, Raman Scattering in Materials Science, Springer Series in Materials Science (Springer, Berlin, Heidelberg, 2000).
- ³¹L. Huang and W. R. L. Lambrecht, "Lattice dynamics in perovskite halides $CsSnX_3$ with X = I, Br, Cl," Phys. Rev. B **90**(19), 195201 (2014).

- ³²F. Brivio, J. M. Frost, J. M. Skelton, A. J. Jackson, O. J. Weber, M. T. Weller, A. R. Goñi, A. M. A. Leguy, P. R. F. Barnes, and A. Walsh, "Lattice dynamics and vibrational spectra of the orthorhombic, tetragonal, and cubic phases of methylammonium lead iodide," Phys. Rev. B 92(14), 144308 (2015).
- ³³ A. M. A. Leguy, A. R. Goñi, J. M. Frost, J. Skelton, F. Brivio, X. Rodríguez-Martínez, O. J. Weber, A. Pallipurath, M. I. Alonso, M. Campoy-Quiles, M. T. Weller, J. Nelson, A. Walsh, and P. R. F. Barnes, "Dynamic disorder, phonon lifetimes, and the assignment of modes to the vibrational spectra of methylammonium lead halide perovskites," Phys. Chem. Chem. Phys. 18(39), 27051–27066 (2016).
- ³⁴M. A. Pérez-Osorio, Q. Lin, R. T. Phillips, R. L. Milot, L. M. Herz, M. B. Johnston, and F. Giustino, "Raman spectrum of the organic–inorganic halide perovskite CH₃NH₃PbI₃ from first principles and high-resolution low-temperature Raman measurements," J. Phys. Chem. C **122**(38), 21703–21717 (2018).
- ³⁵Y. Guo, O. Yaffe, T. D. Hull, J. S. Owen, D. R. Reichman, and L. E. Brus, "Dynamic emission Stokes shift and liquid-like dielectric solvation of band edge carriers in lead-halide perovskites," Nat. Commun. 10(1), 1175 (2019).
- ³⁶H. Seiler, S. Palato, C. Sonnichsen, H. Baker, E. Socie, D. P. Strandell, and P. Kambhampati, "Two-dimensional electronic spectroscopy reveals liquid-like lineshape dynamics in CsPbI₃ perovskite nanocrystals," Nat. Commun. **10**(1), 4962 (2019).
- ³⁷L. M. Herz, "Charge-carrier mobilities in metal halide perovskites: Fundamental mechanisms and limits," ACS Energy Lett. 2(7), 1539–1548 (2017).

- ³⁸ A. Maalej, Y. Abid, A. Kallel, A. Daoud, A. Lautié, and F. Romain, "Phase transitions and crystal dynamics in the cubic perovskite CH₃NH₃PbCl₃," Solid State Commun. **103**(5), 279–284 (1997).
- ³⁹Y. Guo, O. Yaffe, D. W. Paley, A. N. Beecher, T. D. Hull, G. Szpak, J. S. Owen, L. E. Brus, and M. A. Pimenta, "Interplay between organic cations and inorganic framework and incommensurability in hybrid lead-halide perovskite CH₃NH₃PbBr₃," Phys. Rev. Mater. 1(4), 042401 (2017).
- ⁴⁰C. M. Iaru, A. Brodu, N. J. J. van Hoof, S. E. T. ter Huurne, J. Buhot, F. Montanarella, S. Buhbut, P. C. M. Christianen, D. Vanmaekelbergh, C. de Mello Donega, J. G. Rivas, P. M. Koenraad, and A. Y. Silov, "Fröhlich interaction dominated by a single phonon mode in CsPbBr₃," Nat. Commun. 12(1), 5844 (2021).
- ⁴¹H. Richter, Z. P. Wang, and L. Ley, "The one phonon Raman spectrum in microcrystalline silicon," Solid State Commun. **39**(5), 625–629 (1981).
- ⁴²X. S. Zhao, Y. R. Ge, J. Schroeder, and P. D. Persans, "Carrier-induced strain effect in Si and GaAs nanocrystals," Appl. Phys. Lett. **65**(16), 2033–2035 (1994).
- ⁴³T. Kanata, H. Murai, and K. Kubota, "Raman and x-ray scattering from ultrafine semiconductor particles," J. Appl. Phys. **61**(3), 969–971 (1987).
- ⁴⁴G. L. Frey, R. Tenne, M. J. Matthews, M. S. Dresselhaus, and G. Dresselhaus, "Raman and resonance Raman investigation of MoS₂ nanoparticles," Phys. Rev. B **60**(4), 2883–2892 (1999).
- ⁴⁵ A. N. Beecher, R. A. Dziatko, M. L. Steigerwald, J. S. Owen, and A. C. Crowther, "Transition from molecular vibrations to phonons in atomically precise cadmium selenide quantum dots," J. Am. Chem. Soc. 138(51), 16754–16763 (2016).